Progress In Electromagnetics Research B, Vol. 35, 151–166, 2011

NUMERICAL AND EXPERIMENTAL STUDY OF THE HYDRODYNAMIC PHENOMENA IN HETEROGENEOUS SEA SURFACE, EM BISTATIC SCATTERING

S. B. Khadra[1,*], A. Khenchaf[1], and K. B. Khadhra[2]

[1]Ensta Bretagne, E3I2-EA3876 (REMS), 2, rue François Verny, 29806 Brest Cedex 09, France

[2]Interdisciplinary Centre on Climat Change (IC3), Department of Geography and Environmental Management, Faculty of Environment, University of Waterloo, USA

Abstract—In this paper, we will study the influence of nonlinear waves (breaking waves) on the EM signature of a sea surface in bistatic case (forward propagation). Indeed, we will start the temporal numerical analysis of the scattering coefficient σ_{HH} of breaking waves in bi-static configurations. Then, we will show the first experimental validation of the numerical results using well calibrated measurements of precise breaking wave profiles. These experimental measurements have been carried out in X-band in our anechoic chamber (E^3I^2-EA3876-ENSTA BRETAGNE). In this work, we will consider the sea surface as a perfect conductor.

1. INTRODUCTION

Generally, many physical phenomena coexist and affect the electromagnetic wave propagation over a heterogeneous sea surface (Fig. 1); due to the refractive index gradients, roughness of the sea surface, the presence of objects, pollutants, ship wake, areas Coastal. In recent literature, the study of these aforementioned phenomena is generally done separately. To our knowledge, there is no real research that examined the interaction between these phenomena and their contribution to the EM surface scattering containing breaking waves.

This paper focuses on the hydrodynamics phenomena, called the breaking waves. In general, the scattering of an electromagnetic wave by the sea surface can be divided into two distinct phenomena.

Received 20 September 2011, Accepted 11 October 2011, Scheduled 16 October 2011

* Corresponding author: Slahedine Ben Khadra (slah.benkhadra@yahoo.fr).

Initially, there is the scattering of linear waves and secondly, the scattering of breaking waves which cause non-linear phenomena. In our case, we could consider that the ocean surface is geometrically heterogeneous. These phenomena add a component which is not negligible and which is called the non-Bragg diffusion in the total diffusion coefficients. Then in this case, it can be written:

$$\sigma = \sigma_{Bragg} + \sigma_{Non\text{-}Bragg} \tag{1}$$

To date, the Bragg scattering (scattering of linear waves) has been well studied in many papers [1–3]. However, there exists research concerning the non-Bragg scattering only in the mono-static case. For example the work of Holliday et al. [4] shows the existence of the characteristic of a sea peak in the mono-static case for the grazing angle ($\theta_i = -85$ degree). However this characteristic does not exist for the non-grazing angle ($\theta_i = -40$ degree, for example). These results are based on the work of Wetzel [5] which characterizes a sea peak as a rapid variation of the scattering coefficients, and which can exceed 10 dB in a period of 100 ms. This peak can lead to false echo, which can be identified as virtual targets that later disorders the radar detection (false alarm). Therefore, to improve the detection and to reduce false alarm rates, it is important to distinguish between targets and the peak of sea waves generated by breaking waves. For this purpose, we should study the electromagnetic signature of breaking waves, so that we can easily identify the false alarm and then we can filter it.

The surface scattering by breaking waves "non-Bragg" is not enough studied and especially in the bi-static configuration. Therefore, an attempt has been made to study the non-Bragg scattering but in a bistatic configuration (forward propagation: $-90° < \theta_i < 90°$, $-90° < \theta_s < 90°$), (Fig. 2). For this, the scattering coefficient has been calculated for a series of waves of the breaking phase for the different bistatic configurations.

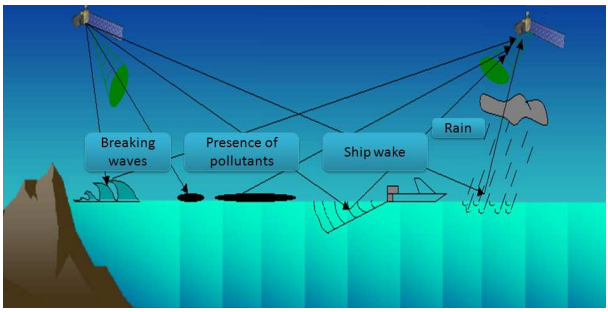

Figure 1. The heterogeneous sea surface.

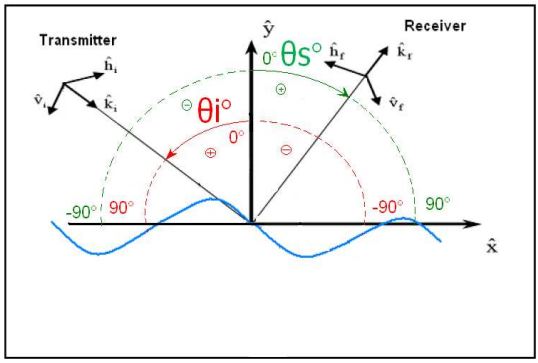

Figure 2. Geometric configuration of the bistatic scattering.

The series of waves are calculated by the simulator LONGTANK [6] developed by the Ocean Engineering Laboratory, University of California Santa Barbara (UCSB). The dispersion of the breaking waves used in this study is more complicated than the rough surfaces because of their complex form. Consequently, this type of surface phenomena cannot be treated by the approximate methods such as KA, SPM, SSA, TSM, WCA [1–3]. We will begin the calculation the scattering of breaking waves by using numerical methods such as the method of the FBM technique (forward-backward) developed by Holliday et al. [7] which gives good results even for multiple profiles (such as breaking waves).

Section 2 describes the breaking waves phenomena. The calculation method of the scattering coefficient is outlined in Section 3. The numerical analysis of the scattering coefficients of the breaking wave for two different construction steps are presented in Section 4. The validation of the numerical results by the experimental radar measurements are detailed in Section 5, and conclusions and recommendations are given in Section 6.

2. BREAKING WAVES

The breaking wave is a dispersion process of the energy which corresponds with the last stage of a wave's life. During this phase, the wave is subject to important transformations in its behavior and structure. When the waves approach a shore, they arrive in waters less than half the depth of their wavelength. Their time period does not change, but their wavelength decreases, as does their speed, however their height increases. When the depth of the coastal water decreases,

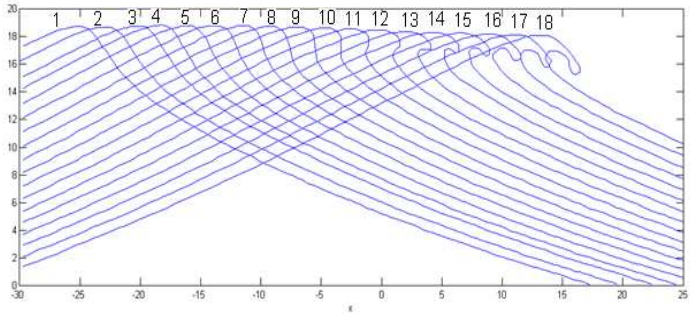

Figure 3. Profile of breaking waves [6].

there is less free space for the water particles situated on the crest of the wave to move around in, therefore the wave breaks.

Recently, it has become possible to numerically simulate these types of waves. Here follows a presentation of the results of one of these simulations which is called LONGTANK [6] (Fig. 3), and which will be used throughout this article as a breaking wave model.

LONGTANK is a hydrodynamic code developed at the University of California, Santa Barbara (UCSB), they have devised a numerical wave basin, for the study of groups of waves, the wave-wave interactions, the deforming of waves, the breaking of waves, and other non-linear effects. Their calculations of wave forms are coherent with experimental measures and observations of the ocean. The 18 waves used in this investigation belong to Case 2.4 (studied by Holliday) [4].

The sequence represents the temporal evolution of a breaking wave with a wavelength of 2.3 m, and during a period of 1.8 seconds. Usually, there exist four types of diffusion mechanism of a breaking wave [8]. A single mechanism with a single trajectory is found and is the diffusion of the crest of the wave, and three mechanisms with multiple (double) trajectories, which are due to the propagation of the electromagnetic waves between the crest and the front side of the waves.

In this case, only the single trajectory is examined since in the profile of the waves. The front side of the waves has been eliminated, as shown by Fig. 4.

3. METHOD OF CALCULATION

In this work, the numerical FBM is used to calculate the scattering coefficient. The FBM has been well-discussed in [7, 8]. Actually, the Integral Equation of the Electric Field (EFIE) for a perfect conductor

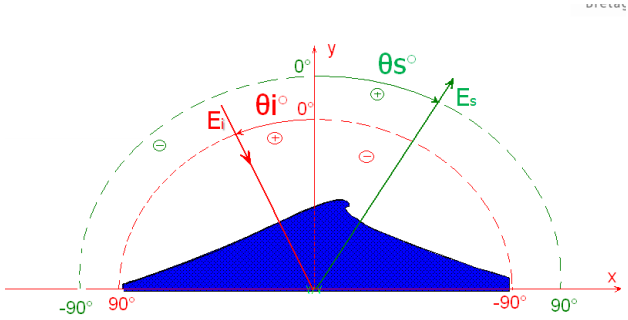

Figure 4. The geometry of diffusion for a breaking wave.

(Equation (2)) is discrete under a matrix form (Equation (3)) by the MoM discretization process [9].

$$\bar{E}(\bar{r}) = \bar{E}_{\text{inc}}(\bar{r}) + i \cdot \omega \cdot \mu_0 \int \bar{\bar{G}}\left(\bar{r}, \bar{r}'\right) \cdot \bar{J}\left(\bar{r}'\right) dS' \tag{2}$$

where $J(r)$ is the induced current on the surface, ω is The radian frequency, μ_0 is permeability of free space, G is the dyadic Green's function for free space and E_{inc} is the incident wave.

$$Z \cdot I = V \tag{3}$$

where Z it is the impedance of the matrix, V is the wave of incidence, and I is the induced current along the length of the rough surface. The FBM method consists of breaking down the Equation (3):

$$I = I_f + I_b \tag{4}$$

$$Z = Z_f + Z_s + Z_b \tag{5}$$

where I_f is the forward component (the current contribution due to the waves propagating forwards), I_b is the backward component (current contribution due to the waves propagating backwards), and Z_f, Z_s and Z_b are respectively, the lower triangular part, the diagonal part, and the upper triangular part of Z.

Using (4) and (5), (3) can now be split into forward propagation and backward-propagation matrix equations, respectively, as follows:

$$Z_s \cdot I_f = V - Z_f \cdot (I_b + I_f) \tag{6}$$

$$Z_s \cdot I_b = -Z_b \cdot (I_b + I_f) \tag{7}$$

This system can resolve itself by iteration:

$$(Z_s + Z_f) \cdot I_f(i) = V - Z_f \cdot I_b \cdot (i-1) \tag{8}$$

$$(Z_s + Z_b) \cdot I_b(i) = -Z_b \cdot I_f(i) \tag{9}$$

The iteration begins by $I_b(0) = 0$.

The algorithm of FBM used in this section is in two dimensions (x, y). An infinite extension is created in the third dimension (z), in which none of the properties vary.

4. NUMERICAL RESULTS

In this part, we will show the numerical analysis of the scattering coefficients variation of two breaking wave profiles, profile number one without crest (Fig. 5(a)) and the profiles number 12 with crest (Fig. 5(b)), which have been generated by the LONGTANK code. In these numerical simulations, we used the Gaussian beam for the transmitted wave.

Usually the breaking wave consists of a crest which can be found between a positive slope and a negative slope. In this first result (Fig. 6(a)), we found out only one crest about 5 dB, which represents the scattering from negative big slope , (Fig. 7(a)). In the second results (Fig. 6(b)) the response of two slopes (Fig. 7(b)) appears in the form of two peaks, nearly 5 dB. And the response of a crest appears in the form of many small peaks [15].

In this first study, we demonstrated that for $\theta_i = 0°$ the simple path scattering from the negative and positive slop of the breaking wave is larger than the scattering from its crest of, for the bistatic configuration. However, Johnson and West proved for the monostatic case and grassing angles in [8, 10] that the scattering from the crest of the breaking wave is more important than the scattering from its slops.

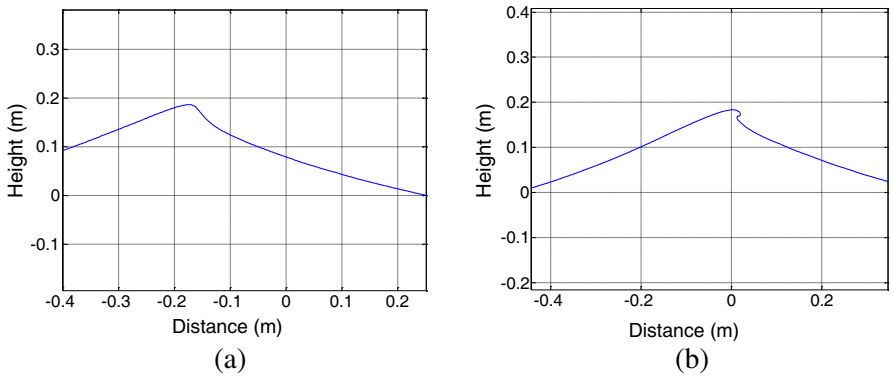

Figure 5. Profile 1 and 2 of breaking waves [6].

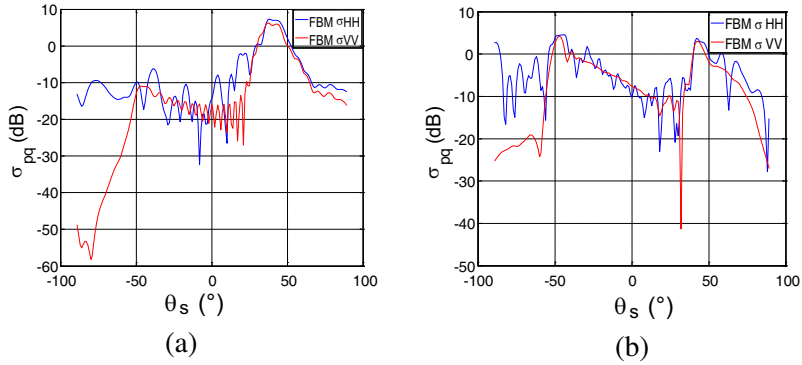

Figure 6. Bistatic scattering coefficients (forward propagation) σ_{HH} and σ_{vv} of profile 1 and profile 12

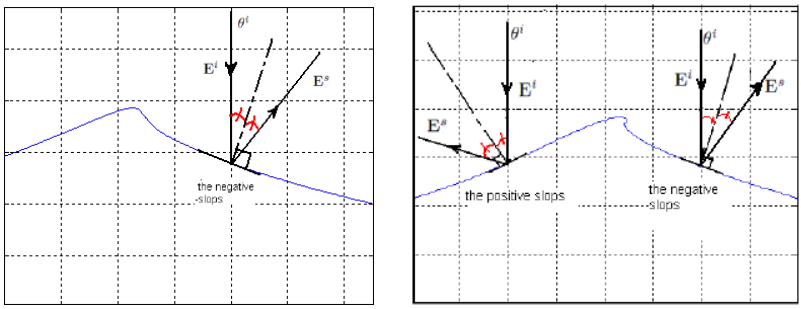

Figure 7. Single trajectory scattering.

As a second step, we will study the temporal variation of the scattering coefficient of a breaking wave. Indeed, we represent the temporal variation of σ_{HH} for the profiles 4, 8, 12 and 16, (Fig. 8).

Wetzel [5] has defined the sea peak as a rapid changing of σ_{HH} exceeding 10 dB in a period of about 100 ms.

For the bi-static configuration ($\theta_i = 0°$ and θ_s between $-42°$ and $-50°$) we found out an increase of σ_{HH}, which is the response of the positive slope of the wave. To understand better this augmentation, we plot evolution of σ_{HH} in function of time. Indeed, we calculate σ_{HH} for the 16 breaking waves profiles (Fig. 9), for the bi-static configuration as follows ($\theta_i = 0°$, $\theta_s = -42°$, $\theta_i = 0°$, $\theta_s = -45°$ and $\theta_i = 0°$, $\theta_s = -50°$).

The Table 1 shows the difference of σ_{HH} (dB) between the profile 12 and profile 3.

Knowing that the time between profile 3 and profile 12 is in order

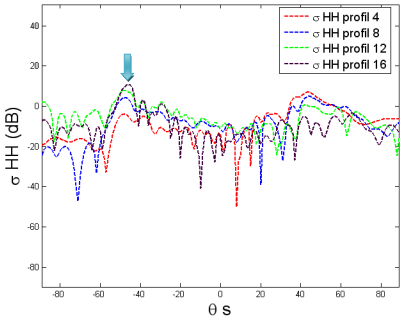

Figure 8. Bistatic scattering coefficients (forward propagation) σ_{HH} of profile 4, 8, 12, and 16 ($\theta_i = 0°$).

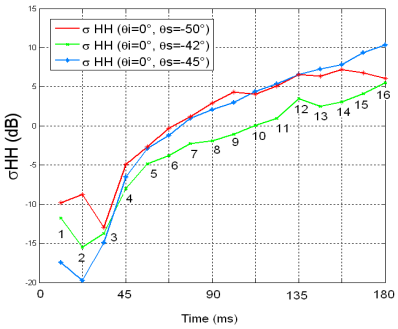

Figure 9. Bistatic scattering coefficients (forward propagation) σ_{HH} of 16 profiles.

Table 1. The difference of σ_{HH} (dB) between the profile 12 and profile 3.

$\theta_i = 0°$	σHH (dB) of profile 12 − σHH (dB) of profile 3
$\theta_s = -42°$	+17.19 dB
$\theta_s = -45°$	+21.53 dB
$\theta_s = -50°$	+19.56 dB

of 100 ms and the difference of σ_{HH} (dB) between these two profile exceeds 10 dB, which satisfies the criterion of Wetzel [5] for a sea peak. Then, we can say that for the bistatic configuration ($\theta_i = 0°$, $\theta_s = -42°$, $\theta_i = 0°$, $\theta_s = -45°$ and $\theta_i = 0°$, $\theta_s = -50°$) we found out the nonlinear effect of a breaking wave which is in the form of a sea peak. Indeed, it is the scattering of the positive slope of the breaking wave, which causes the sea peak [16].

These results are very important. Actually, they prove the significance of the non-Bragg effect (the non linear breaking wave effect) on the EM signature of a sea surface in bistatic case (forward propagation).

5. VALIDATION BY EXPERIMENTAL RADAR MEASUREMENTS

The validation of the numerical simulations have been done in the bistatic measurement facility (Fig. 10), which is located in an anechoic

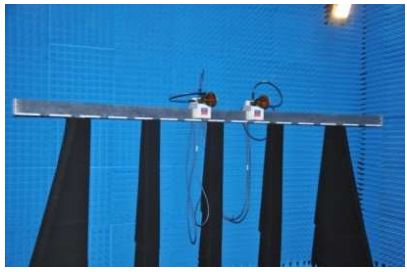

Figure 10. Bistatic radar system.

chamber (7.7 m × 4.4 × 5 m), at E^3I^2-EA3876-laboratory of Ensta-Bretagne.

Before we compare the experimental measurements with the numerical simulation, the bistatic measurements facility has to be calibrated. An important aspect during the calibration process is to filter the noise or errors without losing useful information. An effective calibration technique has been chosen for our anechoic chamber to reduce these errors to acceptable levels and to calibrate the full polarimetric scattering matrix [11–14].

In general, the errors present during the experimental measurements is equivalent to the distortion matrix model or the calibration error model, which relates the ideal scattering matrix of the sample under test to the scattering matrix measured by the network analyzer (NWA) and is represented by four matrices [10]:

$$[M] = [R] \cdot [S] \cdot [T] + [B] \tag{10}$$

Matrix	Description
$[B]$	The empty chamber noise
$[T]$	The transmitter distortion matrix
$[R]$	The receiver distortion matrix
$[M]$	The measured matrix
$[S]$	The ideal matrix

$$[R] = \begin{bmatrix} R_{HH} R_{HV} \\ R_{VH} R_{VV} \end{bmatrix}, \; [T] = \begin{bmatrix} T_{HH} T_{HV} \\ T_{VH} T_{VV} \end{bmatrix}, \; [B] = \begin{bmatrix} B_{HH} B_{HV} \\ B_{VH} B_{VV} \end{bmatrix},$$

The calibration process consists to determine the matrices $[R]$, $[T]$ and $[B]$ and then:

$$[S] = [R]^{-1} \cdot ([S] - [T]) \cdot [B]^{-1} \tag{11}$$

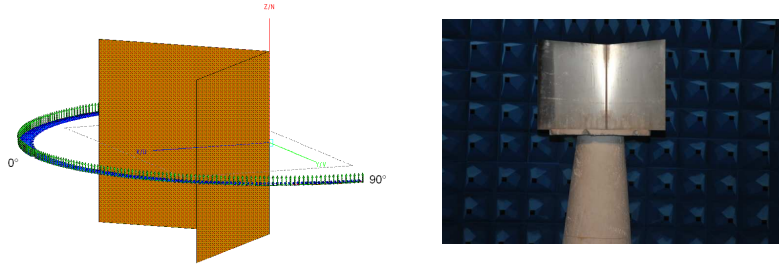

Figure 11. Metallic dihedral.

Wiesbeck and Riegger proposed other representation of the distortion matrices by combining the matrices $[R]$ and $[T]$ as the following:

$$[M] = [C] \cdot [S] + [B]. \tag{12}$$

$$\begin{bmatrix} M_{hh} \\ M_{hv} \\ M_{vh} \\ M_{vv} \end{bmatrix} = \begin{bmatrix} C_{11}C_{12}C_{13}C_{14} \\ C_{21}C_{22}C_{23}C_{24} \\ C_{31}C_{32}C_{33}C_{34} \\ C_{41}C_{42}C_{43}C_{44} \end{bmatrix} \cdot \begin{bmatrix} S_{hh} \\ S_{hv} \\ S_{vh} \\ S_{vv} \end{bmatrix} + \begin{bmatrix} B_{hh} \\ B_{hv} \\ B_{vh} \\ B_{vv} \end{bmatrix}$$

In this case, we have only to calculate the matrix $[C]$ and measuring the empty chamber noise.

Actually, there are different methods or techniques to calibrate the anechoic chamber for the monostatic and bistatic case. These techniques depend on the anechoic chamber. Indeed each measuring system, either in the field or in a controlled anechoic chamber, is different; therefore the method of calibration has to be specially adapted for each case.

In general there are three kinds of calibration:

- Amplitude and phase calibration (Type-1)
- Single polarimetric calibration (Type-2)
- Full polarimetric calibration (Type-3)

For our work, we used the single polarimetric calibration due to its simplicity and convenient results.

To validate our calibration we have done measurements of metallic dihedral (300 cm × 300 cm) (Fig. 11) and trihedral (300 cm × 300 cm) (Fig. 13), in monostatic case and we compare them to the simulation using the physical optics model (Figs. 12, 14).

These results confirm the reliability of the chosen calibration technique.

We firstly show the measurements of profile 12 of the breaking wave (Fig. 15), where the crest is completely formed, using a metallic

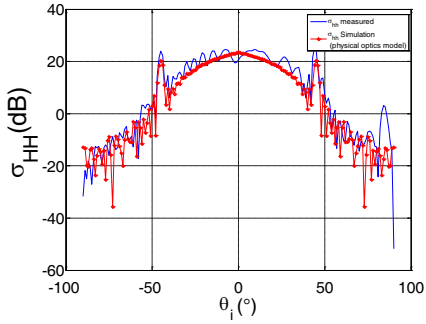

Figure 12. Comparison between the calibrated measurement and the simulated backscattering coefficient σ_{HH} of the metallic Dihedral in mono-static case.

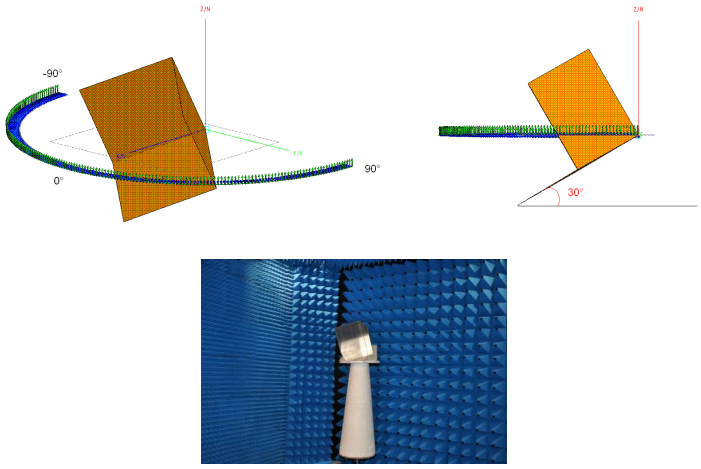

Figure 13. Metallic trihedral.

profile (Fig. 17), in the monostatic and bistatic configuration (forward propagation).

If we consider that geometry of the profile is constant along the axis (Z), it is enough to take a metallic profile with small thickness (3 cm). And thus we can compare our experimental measurements with 1D numerical simulation.

In this validation phase and for the numerical simulation (FBM), plane waves have been considered to enable the comparison between the simulation and the measured data.

An extension is made in the third dimension (z), in which the

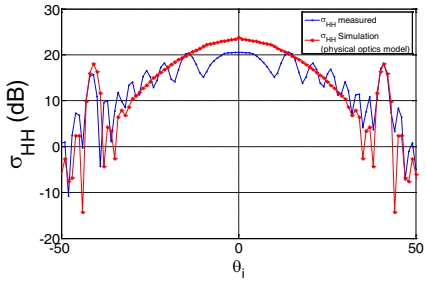

Figure 14. Comparison between the calibrated measurement and the simulated backscattering coefficient σ_{HH} of the metallic trihedral in monostatic case.

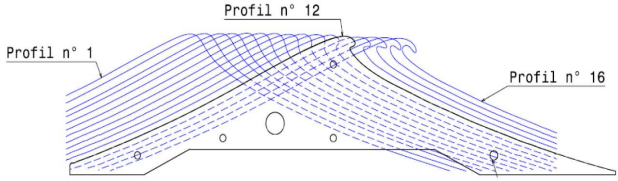

Figure 15. Profile of breaking waves [6].

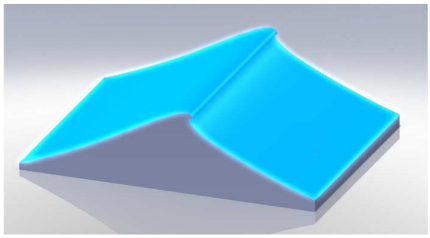

Figure 16. Profile 12 of breaking waves in 3D.

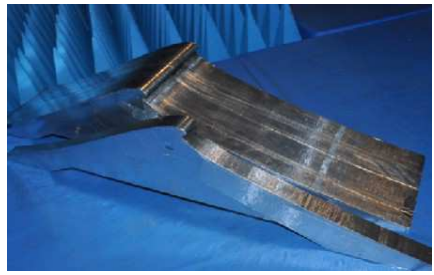

Figure 17. The metallic profile 12 of the breaking wave.

properties of the surface are uniform. Hence we get the profile 12 of wave in 3 dimensions (Fig. 16).

First, we achieved the radar experimental measurement of the breaking wave profile 12 (Figs. 18, 19) in monostatic case.

For the bistatic case, we have chosen the following configuration ($\theta_i = -21°$, $-20° < \theta_s < 60°$), where we can find the response of the breaking wave negative slope (Figs. 20, 21).

We find out that the maximum errors between the measurements

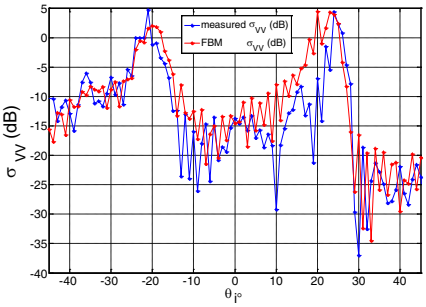

Figure 18. Comparison between the calibrated measurement and the simulated backscattering coefficient σ_{VV} of the metallic wave profile.

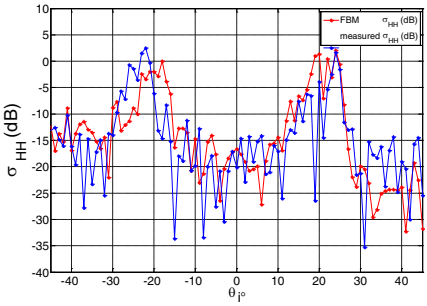

Figure 19. Comparison between the calibrated measurement and the simulated backscattering coefficient σ_{HH} of the metallic wave profile.

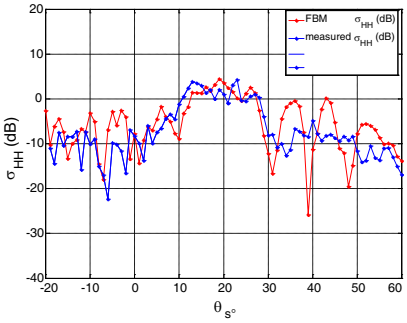

Figure 20. Comparison between the calibrated measurement and the simulated scattering coefficient σ_{HH} of the metallic profile "forward propagation".

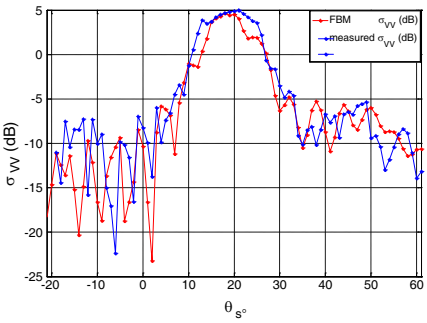

Figure 21. Comparison between the calibrated measurement and the simulated scattering coefficient σ_{VV} of the metallic profile "forward propagation".

and the simulated data in spectral domain is less than 3 dB (Fig. 22), which is an acceptable as preliminary result for the experimental measurements.

These radar experiment measurement validate the simulation results (FBM) in monostatic and bistatic configuration of the breaking wave profile n° 12, where the scattering (simple path) of the breaking wave positive and negative slope is more relevant than the scattering from the crest.

These relevant results show that even the simple path scattering of

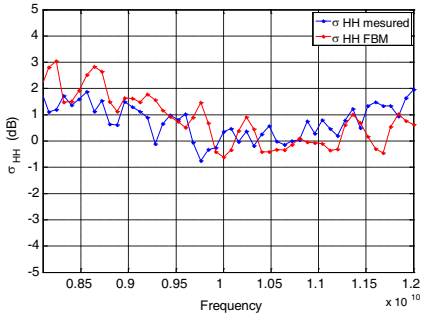

Figure 22. Comparison between the calibrated measurement and the simulated backscattering coefficient σ_{HH} of the metallic profile (profile n° 12 X-band "8 GHz–12 GHz".) "monostatic, $\theta_i = -20°$".

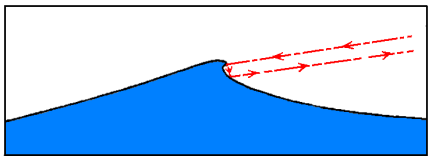

Figure 23. Double bound scattering of the breaking wave crest.

the breaking wave positive and negative slopes generates the sea peak in bistatic case. It should be noted that these sea peaks complicate the ship detection. However, in monostatic configuration and for grassing angles, the sea peaks are produced by the double bound scattering of the breaking wave crest (Fig. 23), D. Holliday [7] and James C. West [10].

With this important result in the bistatic configuration (forward propagation), we can give clear characteristics in terms of scattering mechanism for the sea peaks produced by the breaking waves. And then, we can distinguish between the sea peaks produced either by the searched target or by the breaking wave, which will help us to improve the maritime surveillance system.

6. CONCLUSION

In this paper, we introduced the first study of the breaking wave (nonlinear hydrodynamic effect) in the electromagnetic signature of sea surface for the bistatic configuration (forward propagation).

These results show that for non-grassing angels, particularly for $\theta_i = 0°$ the presence of a sea peak. However, it has been proved that the

sea peak occurs only for the grassing angles monostatic case (Holliday et al. [4]).

We have also demonstrated that the sea peak is due the simple path scattering of the breaking wave positive slope. These results validate the importance of the breaking waves in the calculation of the electromagnetic signature of heterogeneous marine coastal areas in bi-static configuration (forward propagation).

To validate the previous numerical analyses, radar experimental measurements have been carried out in an anechoic chamber for the both configuration (monostatic and bistatic). For this task, the breaking wave profile number 12, which is generated by the LONGTANK [6] code, has been used. These measurements agree obviously with the FBM simulation, where is demonstrated that the scattering from the breaking wave slopes (positive and negative) is larger than the scattering from the peak.

In our future works, we will consider the double bound scattering produced from the front and the crest of the breaking waves. That means the problem will be for 3D surfaces.

REFERENCES

1. Khenchaf, A., "Bistatic scatering and depolarization by randomly rough surface: Application to the natural rough surfaces in X-band," *Waves in Random and Complex Media*, Vol. 11, 61–87, 2000.
2. Awada, A., Y. Ayari, A. Khenchaf, and A. Coatanhay, "Bistatic scattering from an anisotropic sea surface: Numerical comparison between the first-order SSA and the TSM models," *Waves in Random and Complex Media*, Vol. 16, No. 3, 2006.
3. Sajjad, N., A. Khenchaf, A. Coatanhay, and A. Awada, "An improved two-scale model for the ocean surface bistatic scattering," 6–11, IGARSS, Boston, USA, 2008
4. Holliday, D., L. L. DeRaad, Jr, and G. J. St-Cyr, "Seaspike backscatter from a steepening wave," *IEEE Trans. Antennas Propagation*, Vol. 46, 108113, 1998.
5. Wetzel, L. B., "Sea clutter," *Radar Handbook*, M. I. Skolnik (ed.), McGraw-Hill, New York, 1990.
6. Yao, W. P. and M. P. Tulin, "An efficient numerical tank for non-linear water waves, based on the multi-subdomain approach with BEM," *International Journal for Numerical Methods in Fluids*, Vol. 20, 1315–1336, 1995.

7. Holliday, D., L. L. DeRaad, Jr., and G. J. St-Cyr, "Forward-backward: A new method for computing low-grazing angle scattering," *IEEE Trans. Antennas Propagat.*, Vol. 44, 722–729, May 1996.
8. Kim, H. and J. T. Johnson, "Radar image study of simulated breaking waves," *IEEE Transactions on Geosciences and Remote Sensing*, Vol. 40, 2143–2150, 2002.
9. Harrington, R. F., *Field Computation by Moment Method*, IEEE Press, New York, 1993.
10. James, C. W., "Low-grazing-angle (LGA) sea-spike backscattering from plunging breaker crests" *IEEE Transactions on Geosciences and Remote Sensing*, Vol. 40, No. 2, Feb. 2002.
11. Khadra, K. B., "Surface parameter estimation using bistatic polarimetric X-band measurements," Ph.D. Thesis, German Aerospace Centre (DLR), Institute of Radio Frequency Technology, Oberpfa®enhofen, Germany, 2008.
12. Alexander, N. T., N. C. Currie, and M. T. Tuley, "Calibration of bistatic RCS measurements," *Proceedings of Antenna and Propagation Techniques Association (AMTA) 1995 Symposium*, 13–17, Columbus, OH, Nov. 1995.
13. McLaughlin, D. J., Z. Ren, and Y. Wu, "A bistatic polarimeter calibration technique," *IEEE Transactions on Geoscience and Remote Sensing*, Vol. 33, No. 3, May 1995.
14. Sarabandi, K., F. T. Ulaby, and M. A. Tassoudji, "Calibration of polarimetric radar systems with good polarization isolation," *IEEE Trans. Geosci. Remote Sensing*, Vol. 28, No. 1, 70–75, Jan. 1990.
15. Khadra, S. B. and A. Khenchaf, "The bistatic electromagnetic signature of heterogeneous sea surface: Study of the hydrodynamic phenomena," *IGARSS*, 3549–3552, Honolulu, HI, 2010.
16. Khadra, S. B. and A. Khenchaf, "Numerical and experimental study of the hydrodynamic phenomena in heterogeneous sea surface EM bistatic scattering," *OCEANS*, Santander, 2011.